Quantification of slag heap volumes and masses through the use of induced polarization: application to the Castel-Minier site

Nicolas Florsch, M. Llubes, Florian Téreygeol, A. Ghorbani, P. Roblet

Journal of Archaeological Science 38 (2011) 438–451

Contents lists available at ScienceDirect

Journal of Archaeological Science

journal homepage: http://www.elsevier.com/locate/jas

Quantification of slag heap volumes and masses through the use of induced polarization: application to the Castel-Minier site

Nicolas Florsch [a,d,e,*], M. Llubes [b], F. Téreygeol [c], A. Ghorbani [f], P. Roblet [b]

[a] Université Pierre et Marie Curie, Paris, France
[b] Observatoire Midi-Pyrénées, Toulouse, France
[c] IRAMAT-LMC, UMR 5060, Belfort, France
[d] UMMISCO, UMI no209, Institut de Recherche pour le Développement, Paris, France
[e] UMR 7619 Sisyphe, CNRS, Paris, France
[f] Dpt of Mining and metallurgical engineering, Yazd University, Iran

ARTICLE INFO

Article history:
Received 22 December 2009
Received in revised form
20 September 2010
Accepted 23 September 2010

Keywords:
Archaeometallurgy
Slag
Smelter
Induced polarization
Castel-Minier

ABSTRACT

When used for archaeological purposes, geophysical methods are often useful for the exploration, detection and mapping of archaeological remains. In the case of ancient metallurgical activities, slag accumulations form precious mineral records of these activities. Evaluating the volume of slag produced in such locations is an important issue, since it enables an estimate of the amount of metal produced in the smeltery. Unfortunately, slags themselves cannot be easily detected by DC electrical methods. Although they can be easily detected using magnetic techniques, these methods do not allow for an estimate of the quantity of slag, because magnetic fields do not conserve magnetic flux. In the present study we show that the Induced Polarization method (IP) is suited to the quantification of buried slags, provided the slag response has been suitably calibrated prior to the field measurements. The ability to quantify the quantity of slag is based on the quasi-linear relationship between the main IP parameter, i.e., the chargeability, and the slag concentration. This approach provides a new, non-invasive tool for the estimation of the volume of buried slag in palaeometallurgical sites.

In this paper, an application of this technique for the site of Castel-Minier, Ariège, France, is presented.

1. Introduction

Slags represent precious archives of palaeometallurgical activities. They can reveal the firing techniques used to produce metals, and are quantitatively representative of the volumes of processed minerals. Their composition enables determining the know-how of the metallurgist corporations, and the wealth produced by any particular mining claim. This is the reason for which mining and metallurgical archaeologists are particularly interested in the study of these materials.

Amongst the geophysical methods used in archaeology, the magnetic method is traditionally the most suited for the detection of palaeometallurgical remains (Aspinal et al., 2008). Traces of firecraft, particularly concerning all types of ovens, can be detected easily, due to their magnetic properties. In the case of non-metallurgical ovens (pottery and glassware kilns), some ferrous oxides are reduced to magnetite and lead to strong magnetic susceptibilities or thermoremanent magnetisations (Le Borgne, 1960). When metals are processed in ovens and foundries, the metallic and sulphide particles impart their magnetic properties to the remains.

There are two detection modes for magnetic remains, which could be qualified as 'passive' and 'active'. In the most commonly used of these two, the passive mode, the magnetic field produced by the structures themselves is mapped, near the surface. This corresponds to the 'classical' magnetic exploration, for which the canonical anomaly, at moderate latitudes, is clearly identifiable by its bipolar nature. This method is sensitive to induced as well as to remanent magnetisations, and is based on the use of 'proton' or 'optically pumped cesium', or 'flux-gate', etc., magnetometers (see for example Telford et al., 1990 or Scollar et al., 1990). The active method, for its part, involves studying the response of the ground to an alternating magnetic field produced by the device itself. The created field affects only a very small region and produces a secondary magnetic field, which is detected by the same device (a susceptibility meter). This method is only relevant for the induced

* Corresponding author. Université Pierre et Marie Curie, 4 place Jussieu, 75252 Paris, France.
E-mail addresses: nicolas.florsch@upmc.fr (N. Florsch), muriel.Llubes@legos.obs-mip.fr (M. Llubes), florian.tereygeol@cea.fr (F. Téreygeol), aghorbani@yazduni.ac.ir (A. Ghorbani).

0305-4403/$ – see front matter © 2010 Elsevier Ltd. All rights reserved.
doi:10.1016/j.jas.2010.09.027

properties, but allows these properties to be analyzed as a function of the applied frequency (Dabas et al., 1992; Tabbagh and Dabas, 1996; Thiesson et al., 2007), which can then be used to determine the size of the magnetized grains.

Both of these geophysical methods do indeed permit slags to be detected, located and contoured, but the geometric and volumetric characterization of these heaps, in particular in terms of depth, can be achieved only with the greatest difficulties. In the case of the classical approach, this is a consequence of the non-conservative nature of flux: the field strength decreases with the inverse of the cube of the distance, whereas the surface area crossed by the field lines varies with the square of this quantity. Far-reaching hypotheses must then be made, such as, for example, the quasi point-like nature of the source, in order to determine its depth (this is clearly not the case for slags). In the case of the susceptibility method, the sounding depth is constant for a given probe, so that in order to reach a depth of a few meters, an excessively large device would be needed. In any case, this technique only provides the induced magnetization, whereas a large portion of the magnetization of slags is remanent (in particular, thermoremanent or visco-remanent).

The development of alternative methods to enable the quantitative and volumetric characterization of slags is thus desirable. The problem of quantifying the material produced at a given site is a key objective for archaeologists (Decombeix et al., 1998; Domergue and Leroy, 2000). To meet this challenge, the slag is the key element subtending all of the proposed computational systems. Very frequently, the quantification of the mass of rejected material in a slag heap introduces such a degree of uncertainty that the extrapolation of the quantity of iron produced becomes meaningless, as a result of the poor representativeness of the sampled material. Then, the knowledge of the extracted metal is significant in terms of the richness of the mine owner and manager, and permits making a further estimation on the total quantity of metal produced by the mine. Fasnacht (1999) proposed that the slag mass reaches ten times the mass of the extracted metal, while Eschenlohr and Serneels (1991) provided an estimation which probably applies to the present case, and which is much smaller.

Few applications of Induced Polarization (IP) can be found in the literature as far as slag detection is concerned (Florsch et al., 2008). Aspinall and Lynam (1968a and 1968b) were probably the first authors to put forth IP in archaeology, but did not apply it to the survey of slag heaps. Weller et al. (2000) applied IP to the study of a medieval smelting site. Ullrich et al. (2007) have also presented an example of its application to slag prospection, but without providing methodological details.

The work by Nordsiek and Weller (2008) made use of an artificial material including slags from the well-known ancient Harz mines. The authors identified a linear relationship between chargeability and the slag concentration. Meyer et al. (2007) worked on a Spanish site and proposed an estimation of the volume of slag heaps, but not any proper mass estimation.

In the present paper, our contribution consists of investigating the possibilities offered by the induced polarization (IP) method to tackle the amount of slags found in ancient mines in terms of delimitation, volume and mass, and of presenting an application of this method to the site of Castel-Minier, Ariège, France.

2. Site description/archaeological background

When Guillaume Soterel (1340), treasurer of the King of Navarre, and Paul Girardi, a Florentine head miner, wrote a treaty on well mining exploitation and coinage to the attention of their lord (Leroy, 1972), they did not hesitate to use as an example the mine of Castel-Minier in Couserans, of which they wrote: “Sachez que Monsire Rogier de Couminges, seigneur de Saint Geronz, vicomte de Cueran [Couserans], avoit en sa terre, et n’a pas XX vans [1315], la plus franche et plus grande [mine]” (Soterel 1340, fol. 6). Indeed, this site was a very important place for silver production during the High Middle Ages. This position is attested by the conflict which opposed the owners of this mine to the King of France between 1309 and 1349. Concerning the medieval mining potential in the south of France, this conflict had its roots in the intense silver production. According to Girardi, over twenty years, the exploitation of the mine would have produced each year more than 30,000 *livres tournois* or 1.2 tons of silver (Soterel 1340, fol. 6; Verna, 1996). In the fourteenth century, Castel-Minier ranked as one of the largest mines of the French kingdom, providing a huge quantity of lead and silver. Later, whereas the ore deposit was exhausted and the installation vanished, its memory was not lost. Jean de Malus, mint master of Bordeaux, wrote a treaty on the mineral richness of the Pyrenees, in which Castel-Minier is presented as an important source. The same author mentions that a foundry was established inside the castle (Malus, 1990). The geochemical survey undertaken on this area of the site revealed a high concentration of lead in the soil and a similar pattern for zinc and copper (Téreygeol et al., in press). The first archaeological excavation carried out in 2003 resulted in a widening of the thematic and chronological fields of interest. Castel-Minier appears as a milestone for the understanding of the silver mining techniques during the High Middle Ages (12th–15th centuries AD) in the south of the French kingdom. The data related to this site represents a valuable supplement to the work conducted at Melle for the early Middle Ages (Téreygeol, 2002), at Brandes-in-Oisans for the period of the 11th–13th centuries AD (Bailly-Maitre and Bruno-Dupraz, 1994), and at Pampailly for the end of the Middle Ages (Benoit, 1997).

Castel-Minier was also the place of an important iron production between the 14th and 16th centuries, a production which, without the agreement of 1348/1349, would not be easily findable in the archives (Verna, 2001). At this time, the community exploiting the well-known iron mine of Rancié made an agreement with the Viscount of Couserans. The former provided iron ore in exchange for the right to produce charcoal in the forests of Couserans. This agreement was subsequently renewed until the end of the 18th century.

The surveys undertaken at the site quickly led to the localization of two slag heaps. The excavation which followed made it possible to characterize an obvious use of hydraulic force for iron and steel production. According to geographical space and chronology, it was clear that we had excavated an unknown iron plant from the archaeological point of view: a ‘*mouline*’. This type of factory is specific to the centre of the Pyrénées, and is characterized as a hydraulic forge. However, we do not know if this term indicates a hammer and/or blower driven by a waterwheel. The stratification of the layers shows that this *mouline* was established at the beginning of the 14th century and was in use until the second half of the 16th century. By chance, the site as a whole is completely closed down and nothing, especially not the rising of a forge ‘à la Catalane’, came to disturb this iron and steel factory. Taking advantage of the existing layout of the site, in particular of one water channel supplying silver ore-mills and the silver refining furnace, contractors erected a *mouline* at the foot of the Castle of Castel-Minier.

As it is obvious that Castel-Minier represents an exceptional combination of silver, lead and steel production, its study must be exemplary and not leave anything unexplored. In agreement with the French archaeological authorities, we have chosen to explore methodological developments in the archaeometric field while maintaining our goal of the archaeological understanding of metallic production systems in the Middle Ages. The five directions

we are currently developing in the context of an inter-disciplinary project are: geochemical surveys (Téreygeol et al., in press), geophysics (Bonnamour et al., 2007), setting up a field laboratory for slag analysis *in situ* (Téreygeol, 2009), metallographic studies of iron artefacts (Dillmann et al., 2006) and chemical determinations pertaining to the diffusion of ferrous products (Leroy, 2010). These direction help guide the choices made during the excavation. They also help us place the production at this site in the context of a technical history, as well as in the context of the medieval economy of southern France.

3. A geophysical method to prospect slags: the induced polarization (IP) method

3.1. Principles of the method

The IP method is related to electrical methods, and most of the concepts and arrays used for electrical methods can be extended to IP, following small adaptations. It is directly related to the complex conductivity (or its inverse resistivity), in which Ohm's law is written under a complex form derived from Maxwell's equations (see for instance Guéguen and Palciauskas, 1992, or Schön, 2004):

$$\vec{j}^{*} = (\sigma + i\omega\varepsilon)\vec{E} = \sigma^{*}\vec{E} \tag{1}$$

where $\varepsilon = \varepsilon_r\varepsilon_0$.

Here $\varepsilon_0 = 8.854\cdot10^{-12}$ Fm^{-1} is the permittivity of vacuum, $\vec{E}$ is the electric field in Vm^{-1}, and ε_r is the 'relative' dielectric constant. Generally speaking ε is complex and frequency dependant, so it can be written as:

$$\varepsilon(\omega) = \varepsilon'(\omega) - i\varepsilon''(\omega) \tag{2}$$

The petrophysical parameter involved in IP studies is the complex form of the conductivity, that is:

$$\sigma^{*} = \sigma + i\omega\varepsilon'$$

or its inverse:

$$\rho^{*} = \frac{1}{\sigma^{*}}. \tag{3}$$

The additional parameter noted ε'' is used to show losses in displacement current, a phenomenon of weak importance at low frequency, at the opposite end of the radio frequency range. It can be disregarded in our case.

Wenner, dipole–dipole, etc. arrays are thus deployed in the field, although various precautions must be taken, particularly in order to reduce electromagnetic coupling (Millett, 1967; Dey and Morrison, 1973; Hohmann, 1973; Wait and Gruszka, 1986). Such coupling effects represent the limitations of the method, and must be carefully taken into account (Wynn and Zonge, 1977). Recently, Ingeman-Nielsen and Baumgartner (2006) provided tools for the modelling of these effects, whereas Ghorbani et al. (2009a) developed inversion techniques which take coupling effects into account.

When compared to electrical methods, IP adds a temporal (equivalently, frequential) dimension to the physics of the measurement. Nonetheless, it is not concerned with frequencies higher than the order of 10 kHz, beyond which induction phenomena, *sensu stricto*, become predominant.

In the so-called time-domain mode, the current is injected as for an electrical method and is then suddenly cut-off, and the ground potential is measured after this cut-off. In practice, an alternating current is used, since it permits, in particular, an improved reduction in spontaneous polarization. Following the cut-off, the shape of the voltage potential, which initially drops very rapidly with respect to its value as measured during the injection, then decreases exponentially. Fig. 1 illustrates the main characteristics of these signals: the data shown is the decreasing potential $V(t)$.

In the Spectrally Induced Polarization mode, a sinusoidal current is injected and the measured voltage is referenced in terms of amplitude and phase (Fig. 2). A few decades ago, it was customary to refer to this mode as Frequency Induced Polarization, indicating cases in which two square-wave signals were used at two different frequencies (see for example Telford et al., 1990).

Mathematically, it is possible to switch between the data from one or the other of these modes, by means of the Fourier or Laplace transforms. In practice, this conversion is not always straightforward. Indeed, in the case of the spectral method, the emission

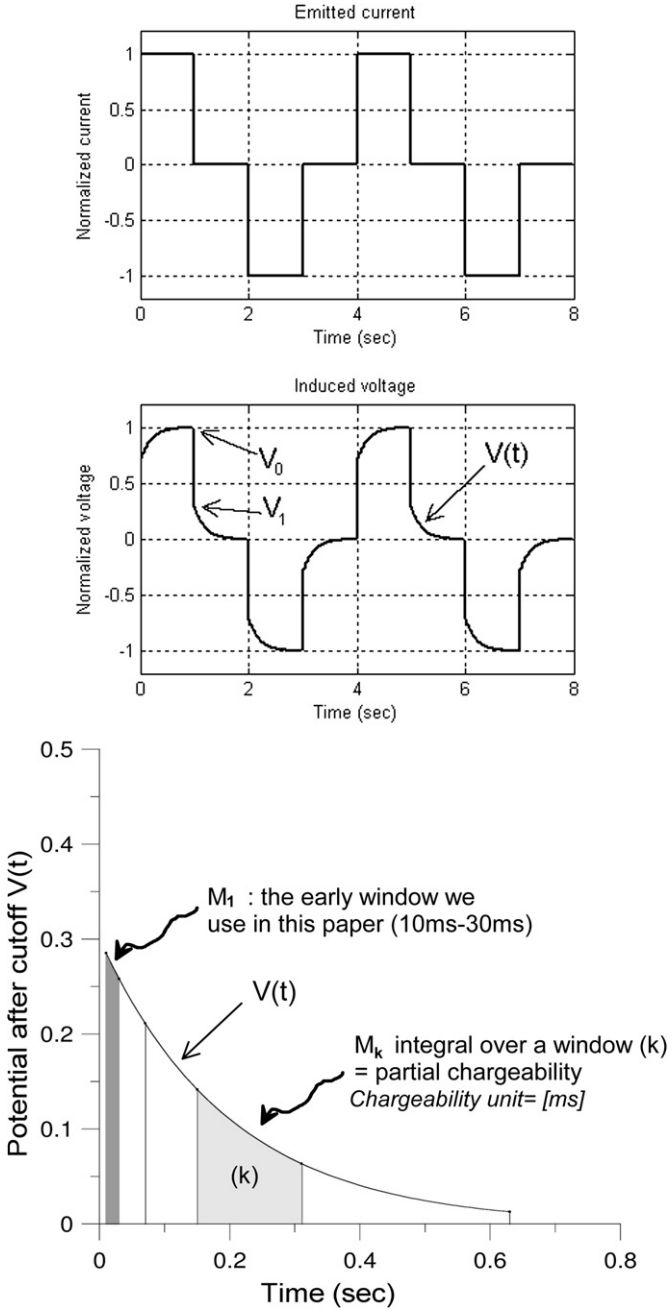

Fig. 1. Signals and observables used in time-domain induced polarization.

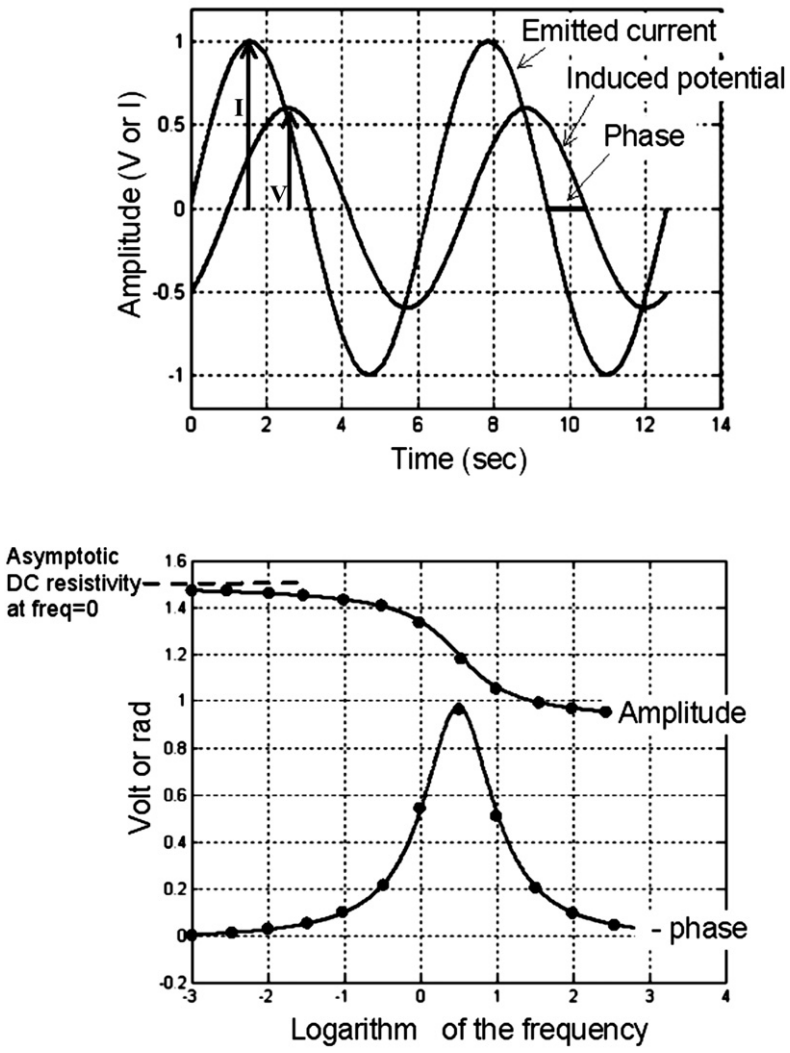

Fig. 2. Signals and observables used in spectral induced polarization.

spectrum of the current is composed of rays whose amplitude is constant over a large range of frequencies (SIP is considered to cover the spectrum between 0.001 Hz and 12 kHz), whereas in the time domain, the amplitude decreases rapidly with frequency, and the range of frequencies covered is far more restricted, typically from ¼ Hz to 64 Hz (see for example Ghorbani et al., 2007).

From the spectral point of view, the classical DC electrical method corresponds to a zero frequency: this representation illustrates the fact that IP is an extension into the frequency (or time) domain of the DC method. Whereas the electrical method leads to the determination of just one parameter (resistivity), the induced polarization curves lead to several additional degrees of freedom, according to the model used. Moreover, the addressed physical phenomenon itself is extended, since it involves, in addition with respect to the case of the DC resistivity, a phenomenological electrical permittivity.

There are several physical origins of the polarization phenomenon, and these often have overlapping spectral domains: it is not always possible to clearly identify the origin of the measured signals. The review published by Luo and Zhang (1998) considers the most frequently discussed processes. Practically, most of the soil and underground materials show some response that falls within IP effects, but only (i) the disseminated particles with metallic conductivity, and (ii) some exceptional pollutions (with or without metal) lead to an important effect similar to the one observed for slags. Most recent developments addressed the ability of IP to discriminate clays, cracks in rocks, hydraulic conductivity, salinity, etc. (see for instance Cosenza et al., 2007; Ghorbani et al., 2008; 2009b; Titov et al., 2009; Revil and Florsch, 2010 for additional readings and references about these applications).

From the point of view of the physical phenomena involved, or by referring to Maxwell's equations, the analysis of the induced polarization is similar to the study of the role of dielectric permittivity. In the general case, permittivity is a tensor with complex values, which includes the superimposed contributions resulting from several phenomena, for which the effective (experimental) expression depends on the frequency range under consideration.

At frequencies considered to be low (typically in the range $[10^{-3},10^{4}]$ Hz), two main types of polarization can be distinguished: (1) a so-called 'membrane' polarization, at the upper end of the frequency spectrum, related to the behaviour of the electric charge in the vicinity and between clay plates (the notions involved are those related to the Stern and diffuse layers), and (2) a so-called

'electrode' polarization, which has the same fundamental origin, but occurs in the vicinity of particles having electron conductivity properties (typically metals, most sulfides, magnetite, ilmenite, cassiterite, and also graphite).

We are convinced that the signals associated with slags result from what is referred to as 'electrode polarization', in the presence of particles with metallic conductivity. The classical illustration of this phenomenon, which can be found in Telford et al. (1990), for example, makes use, on one hand, of micro-hydrological blocking of the electrolytes, and, on the other hand, of a metallically conductive particle blocking a porous gap. Although not fully recognized, no objections have been raised to this model. Nevertheless, it is possible that no blocking at all is needed to produce this phenomenon.

Magnetite is a strong candidate for iron metallurgy slags, since the response of magnetite is approximately half as strong as that of sulfides (see Schön, 2004). Carbon could also play a role in cases where significant traces of charcoal are present. To date, the IP signal carrier in slags has not been identified.

3.2. Mathematical models of the elementary IP response in the time and frequency domains

A summary of the models used in the frequency domain is proposed, for example, by Dias (2000), who provides illustrations of not less than twelve of these, with their equivalent electrical circuits. Debye's model is the simplest, and, in physical terms, it corresponds to a simple relaxation. It is a special case of one of the most commonly used models: the so-called 'Cole–Cole model' (Cole and Cole, 1941), in which the constant (c) is equal to 1. The corresponding time-domain functions are described by Yeung and Shin (1991).

The plethora of models proposed seems to result from the underlying difficulty inherent to this phenomenological approach. Although it is not the purpose of the present paper to discuss these difficulties, it is important to point out that they are perhaps related to the superposition of several types of polarization phenomena, as discussed above, as well as to the superposition, for a given type of model, of its characteristic time constants, which are certainly associated with fractal properties. One remarkable unifying approach, at least mathematically speaking, appears to be that of Shin and Yeung (1988), who show that many known (experimentally or according to various theories) spectral responses are solutions to a non-linear differential equation they propose. However, since this useful theory is not used in the context of this paper, we will limit ourselves to this brief mention of it.

In the simplest of the models, that of Debye, the spectral response is written:

$$\rho = \rho_0\left[1 - m\left(1 - \frac{1}{1 + i\omega\tau}\right)\right], \tag{4}$$

where ρ is the resistivity function at the angular frequency ω, ρ_0 is the DC resistance, m is a parameter called the electrical chargeability, and τ is a characteristic time constant.

With this model, and if it is assumed that the current is injected for a reasonably long period of time before cut-off, the ensuing current decay following the latter can be written as:

$$V(t) = V_1 e^{-t/\tau} = V_0\frac{V_1}{V_0}e^{-t/\tau} = V_0 m e^{-t/\tau} \tag{5}$$

where V_0 is the (stabilised) voltage measured just before, and V_1 the voltage measured just after the cut-off (the latter implies: after a time corresponding to that of the numerical sampling interval following the cut-off). In practice, since the current is alternating, this is accounted for by adding copies of this function, shifted by half the signal period, and multiplied by a (+) or (−) sign, according to the cycle.

The Cole–Cole model is written (with $c = 1 - \alpha$):

$$\begin{aligned}\rho &= \rho_0\left[1 - m\left(1 - \frac{1}{1 + (i\omega\tau)^c}\right)\right] \\ &= \rho_0\left[1 - m\left(1 - \frac{1}{1 + (i\omega\tau)^{1-\alpha}}\right)\right]\end{aligned} \tag{6}$$

The corresponding temporal curve requires more complicated functions, and the interested reader may refer to Pelton et al. (1978) and Hilfer (2002).

The Cole–Cole model is widely used in IP studies since it can be obtained by superimposing Debye expressions for a specific distribution of time constants, which follow a so-called Cole–Cole time constant distribution, not described here. This law, which appears to be *ad hoc*, is not very different from a log–normal relationship (see Cole and Cole, 1941; Fuoss and Kirkwood, 1941).

This notion of a superposition of time constants is intellectually convincing, with the subsoil response then being represented by the superposition of simple relaxations, with time constants distributed over a given domain, at the microscopic level, but also by the superposition in different subsoil compartments (at the metric scale, for example). This is one of the reasons for which there is such a large number of models, and the success of the Cole–Cole model probably lies in its simplicity and the good degree of approximation which it allows (which does not mean that it is universally applicable).

3.3. Practical quantities measured by induced polarization and model estimations

In the spectral domain, the measured quantities are the amplitude and phase of the response to a sinusoidal injected current. These two quantities can be represented as a function of frequency, or using an Argand diagram, with the real part along the abscissa and the imaginary part along the ordinate axis, and the frequency aligned with the parametric curve. After selecting a type of response (from a model), an adjustment enables the model constants to be determined, for example the constants ρ_0, m, τ and c for the Cole–Cole model. Very often, simplified parameters are chosen (defined on the basis of the DC resistivity ρ_{DC} and at a given frequency ρ_{AC}), such as the 'frequency effect' defined by Telford et al. (1990):

$$\mathrm{FE} = \frac{\rho_{DC} - \rho_{AC}}{\rho_{AC}} \tag{7}$$

or alternatively by

$$\mathrm{FE} = \frac{\rho_{LF} - \rho_{HF}}{\rho_{LF}} \tag{8}$$

when using a low frequency 'LF' and a higher frequency 'HF'. This value can also be expressed in percentages, and is then referred to as the 'Percent Frequency Effect' (PFE).

These are practical quantities for mineral prospection, where the 'Metal Factor' is also used, for which one commonly used definition is the one proposed by Telford et al. (1990):

$$\mathrm{MF} = 10^3 \cdot \frac{\mathrm{PFE}}{(\rho_{DC}/2\pi)} \tag{9}$$

It is important to note that some authors use alternative definitions (see for instance Parasnis, 1997).

In the time domain, the decay curve following the current cut-off is used. Traditionally, partial chargeabilities are then derived from this, over a time interval $[t_i,t_{i+1}[$, by:

$$M_{i,i+1} = \frac{1}{V_0}\int_{t_i}^{t_{i+1}} V(t)\mathrm{d}t. \quad (10)$$

When the integral covers the longest possible period of time (from cut-off until a new injection), one often refers to a so-called 'total chargeability'.

For the Debye model, for which $V(t) = V_0 m e^{-t/\tau}$, a rapid calculation leads to the following result:

$$M_{i,i+1} = m\tau\left(e^{-t_i/\tau} - e^{-t_{i+1}/\tau}\right). \quad (11)$$

For the Cole–Cole model, the same calculation leads to a more complex equation, provided in Appendix.

More rigorously, the actual form of the IP signal injected into the arrays, i.e., a square pulse, should be taken into account. In reality, the measured signal is (see for example Ghorbani et al., 2007):

$$S(t) = V(t) - [V(t+T/4) + V(t+T/2)] + [V(t+3T/4) + V(t+T)] - [V(t+5T/4) + V(t+6T/2)] + \ldots \quad (12)$$

It can, however, be estimated that after 10τ there is only a negligible memory of past signals, since $e^{-10\tau/\tau} = 4\cdot10^{-5}$, so that the number of on-periods to be taken into account in the model would be $N_{\text{créneaux}} = 10\tau/T$, where T is the period of the emitted signal.

3.4. Adapting a field strategy for slag heap survey and calibration of the method

Working in the frequency domain is definitely richer in terms of the collected information than working in the time domain. Unfortunately, it is time consuming, more restrictive, and fastidious as far as the field implementation is concerned. Our aim was to validate a rapid IP tool for use in the field, and we thus set out to use the time-domain method together with a classical IP/resistivity device (the Terrameter SAS1000 from ABEM).

The question then is: how should one proceed in the time domain rapidly, when this implies measurements with time constants of the order of 1 s, which is the order of time constant in the case of slags?

For the Debye model, the total chargeability is $M = m\tau$. Normally, measurements lasting several seconds would be needed to determine this chargeability; however, it is important to investigate the possibility of using shorter measurements, in order to maintain the advantage of this approach over that of the frequency domain.

Let us consider the expression given as Equation (11) in the particular case where $t_1 < t_2 << \tau$. Under this assumption, and using a short asymptotic development, the following first order approximation is found:

$$M_{t_1,t_2} = m(t_2 - t_1) = m\Delta t \quad (13)$$

When the same assumption for $t_1 < t_2 << \tau$ is applied to the Cole–Cole model, the same result is found (details of the calculation are provided in Appendix).

The partial chargeability of an early window is thus proportional to the parameter (m) of the relatively general Cole–Cole model. This parameter, also called chargeability, varies between 0 and 1, and can be related to the number of polarizable particles in the medium (see for example Ghorbani et al., 2007).

In order to ensure the condition $t_1 < t_2 << \tau$, there is an obvious advantage in considering only the first integration windows, although the risk of a possible transient signal which could arise just after the cut-off must be avoided. This is the procedure that we propose here. On the field, and for the calibration procedure below, we used a time window of [10 ms, 30 ms]; the justification for this is found in Appendix.

3.5. Calibration of the method

The calibration was aimed at associating a given concentration of slag with a value of the chargeability. To be effective, the same procedure (IP emitted signal, chargeability windows) must be used in the laboratory rather than in the field. The experimental device is described in Fig. 3. In order to comply with the scaling factor, of the order of 10 in view of the electrode arrangement used in the field, the slags were crushed, and only the fraction sized between 2 and 4 mm was used. The procedure consists of first mixing the slags up to 40% (in mass) with neutral earth, and of subsequently removing controlled masses of slag and replacing the removed mass of slag by the same mass of neutral earth, until only a small amount of slag remains in the tank.

We verified the robustness of this approach by modifying the distribution of slags in the container (by increasing the concentration at the bottom, for example), or by carrying out measurements for an equivalent mass with a set of larger slags. The chargeability appeared very robust with respect to the slag distribution. This feature can be linked to the known robustness of the IP parameters with respect to the topography of the field: except for the resistivity itself, all of the parameters of the Cole–Cole model

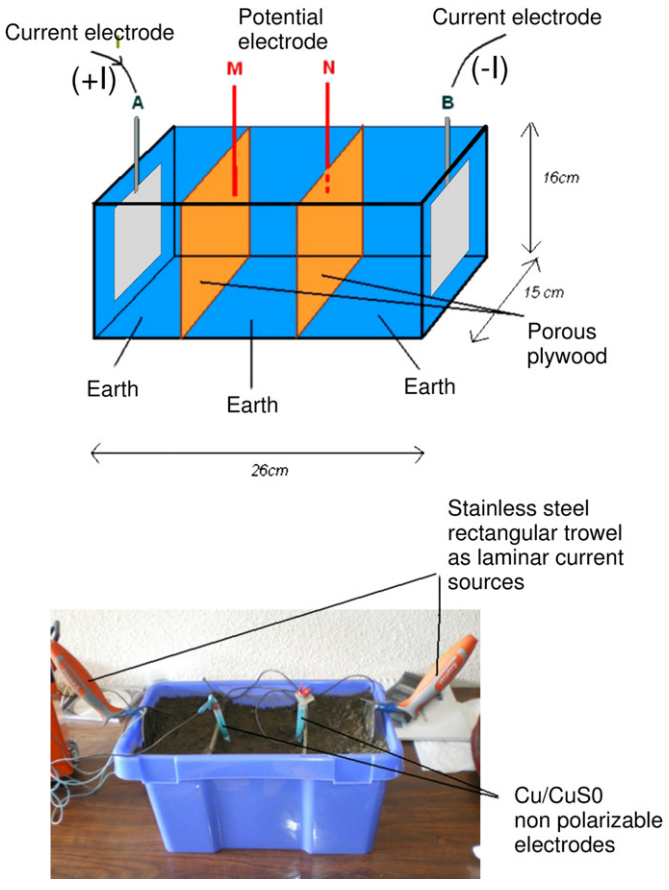

Fig. 3. Plastic tank system for laboratory measurements of the slag IP response.

have this property. This is not surprising as far as the time relaxation constant is concerned, but the robustness of the chargeability is less intuitive.

The device used for this procedure was a Terrameter SAS1000, the same as the one used in the field. The smallest possible voltage was used. If this precaution had not been taken, the change of scale would have led to excessive current densities, with the risk of non-linearities associated with possible redox transformations. The duration of the injection corresponding to a positive pulse is 1 s. We chose from the device outputs the partial chargeability of the time window $[t_1, t_2] = [10\text{ ms}, 30\text{ ms}]$

$$M_{t_1,t_2} = \frac{1}{V_0}\int_{10\text{ms}}^{30\text{ms}} V(t)\mathrm{d}t \cong m(t_2 - t_1) = m\Delta t = m\cdot 20\ \text{ms} \tag{14}$$

(that is, the same as in the field, otherwise it would not be possible to convert the field chargeability into a value corresponding to the percentage of slag mass) from which the value of (m) can be derived. The above times are based on the assumption of $t_1 < t_2 << \tau$, which validates the above equality for the Cole–Cole model, since the spectral measurements have shown that the time constant is greater than several hundreds of milliseconds.

The results of this calibration are provided in Fig. 4. They indicate an affine relationship with a correlation coefficient close to 1. A 'background' signal can be observed, which probably originates from the soil response in the absence of slag. Indeed, according to Seigel et al. (2007), the inventor of the method, Conrad Schlumberger himself (Schlumberger, 1920), is said to have been exasperated by the discovery that all mediums have a non-zero residual response, which he believed, until theoretical and instrumental progress proved the contrary, to imply that his method was invalidated. The Russian school, which, in the footsteps of Schlumberger, developed induced polarization, then showed that this minimum background level was low and limited, so that such calibration could allow it to be taken into account. The reader interested in the detailed history of this method should refer to the above-referenced paper by Seigel et al. (2007).

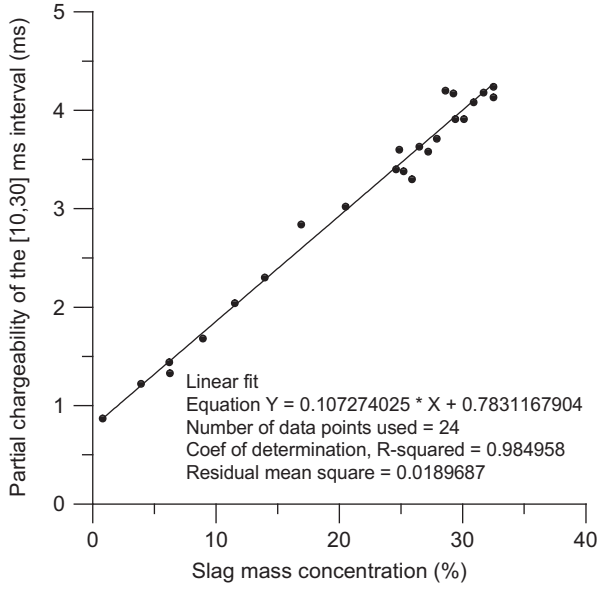

Fig. 4. Calibration curve linking the partial chargeability to the slag content. Experimental relationship showing the affine dependence between slag mass concentration and instrumental chargeability, as obtained with the laboratory tank procedure.

This law can thus be expressed by a relation of the form:

$$M_{t_1,t_2} = \alpha C + \beta \tag{15}$$

where C is the concentration of the slags (in this case, mass). Its inversion is immediate:

$$C = \frac{M_{t_1,t_2} - \beta}{\alpha}. \tag{16}$$

The calculation of the uncertainty on C for a field application must take several factors into account:

- the error in the fit factors α and β, where $M_{t1,t2}$ are the chargeabilities measured on samples analyzed in the laboratory,
- the error in the field measurement of $M_{t1,t2}$, resulting from the use of the formula.

The latter is a composite error: it arises not only from the measurement error, but also from the uncertainty resulting from the geophysical operating sequence. More precisely, the 'raw' chargeabilities are apparent chargeabilities, as is the case, with the same scaling properties, of apparent resistivities. Only after inversion do real chargeabilities become accessible. However, as for the case of resistivities, again, these are spatially smoothed and affected by uncertainties specific to the inversion, and to the 'equivalence laws', well known in geoelectrical techniques.

4. Results – application to the Castel-Minier heap

4.1. Preliminary investigation using SIP

The area where the first experimental profile was established was chosen following the results obtained from the magnetic exploration activities reported by Bonnamour et al. (2007). In order to maintain a certain degree of generality and optimise this initial exploratory phase, we chose, at the beginning of the study, to implement spectral induced polarization along a profile crossing two heaps detected by magnetic survey. This methodology was more time consuming than time-domain exploration, but provided a greater wealth of information for the beginning of the study. The apparatus used was a SIP-FUCHS device from the Radic Research company (www.radic-research.de) which allows measurements between 1/1000 Hz and 12 kHz. It makes use of optical fibres in order to minimize electromagnetic coupling effects, which are always troublesome in induced polarization measurements (see Ghorbani et al., 2009a).

The electrodes were all of the non-polarizable type, made with the $Cu/Cu^{++}SO_4^{--}$ pairs. We constructed these with porous ceramic cones, normally intended for the supply of water to flower pots (Fig. 5). The measured profile traverses two heaps identified by the magnetic method, as shown in Fig. 6.

Fig. 7 shows the results obtained, in the form of sets of amplitude and phase curves along this profile, as well as the results of laboratory measurements carried out directly on a run-of-mine sample taken from the centre of one of these heaps (which corresponds to a slag 'concentrate' when compared with the terrain's situation, in which the slags are more strongly mixed with soil). All of the amplitude profiles decrease as a function of frequency, but do not reveal – apart from a very slight inflexion – the presence of the heaps. On the other hand, the phase profiles have a specific, bell-shaped response centred at 1 Hz. The latter is hardly apparent between the heaps; however, it corresponds to a doubling of the phase, from 40 mrad to 80 mrad, in the vicinity of the most well-confined of these.

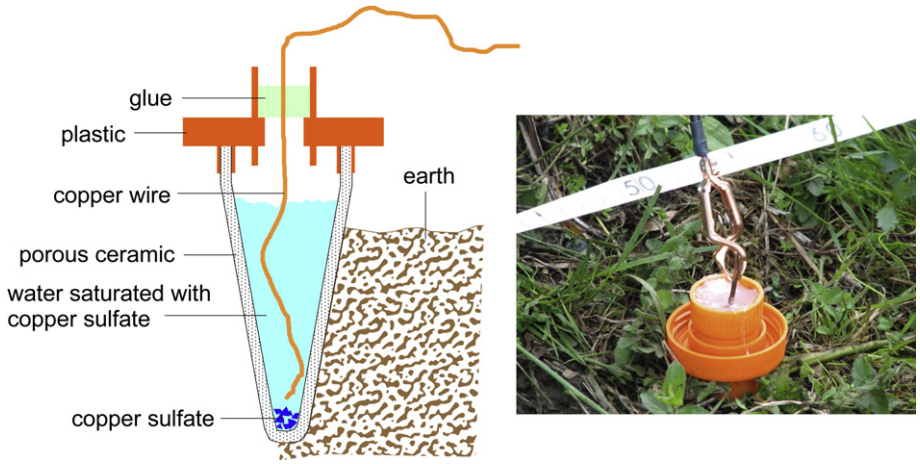

Fig. 5. Non-polarizable electrode used for the induced polarization measurements.

When a Cole–Cole model is fitted to the bell-shaped part of the curve (limited to the range from 0.1 Hz to 10 Hz), the corresponding time constant is found to lie, with certainty, between 500 ms and 2 s (the uncertainty arises, in particular, from the influence of the edge of the spectrum, where the phase increases rapidly which could include a non-specific response to clays and/or a Maxwell–Wagner type of response). It should be noted that these relaxation times are of the same order of magnitude as the constants known for scattered sulfide mineralizations.

4.2. Mapping and tomography in the time domain

At this stage, we applied the theory developed in Section 3.4 of the present paper by using the partial chargeability between 10 ms and 30 ms, converting it to the chargeability (m), and then, by using the calibration results, to the density of slags.

The mappings of both the DC and IP measurements are undertaken by using the same Wenner Beta configuration (or dipole–dipole with $n = 1$). The length of the array is then 3 m. The spacing between measurements is 1 m along the x axis and 1.5 m along the y axis, and the data centred on the centre of the array. This grid spacing should avoid aliasing and the Wenner Beta configuration has been preferred to the Wenner Alpha because it is much less sensitive to the 'ghost' phenomenon (see for instance Panissod et al., 1998).

The 2D ERT in the RES2DINV frame has been measured 'by hand', that is by using single wires in order to minimize the EM coupling. The array is a dipole–dipole one with $a = 0.5$ m and only

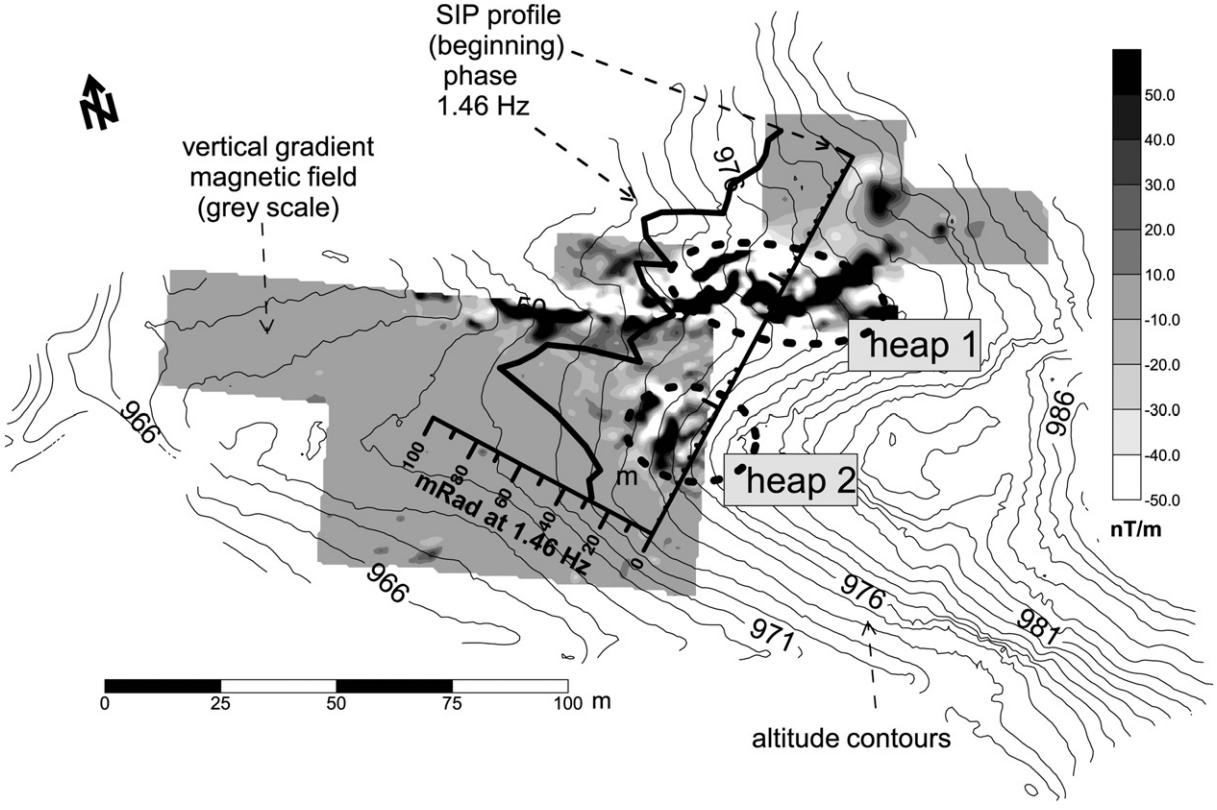

Fig. 6. Position of the SIP profile on the magnetic map prior to the IP study.

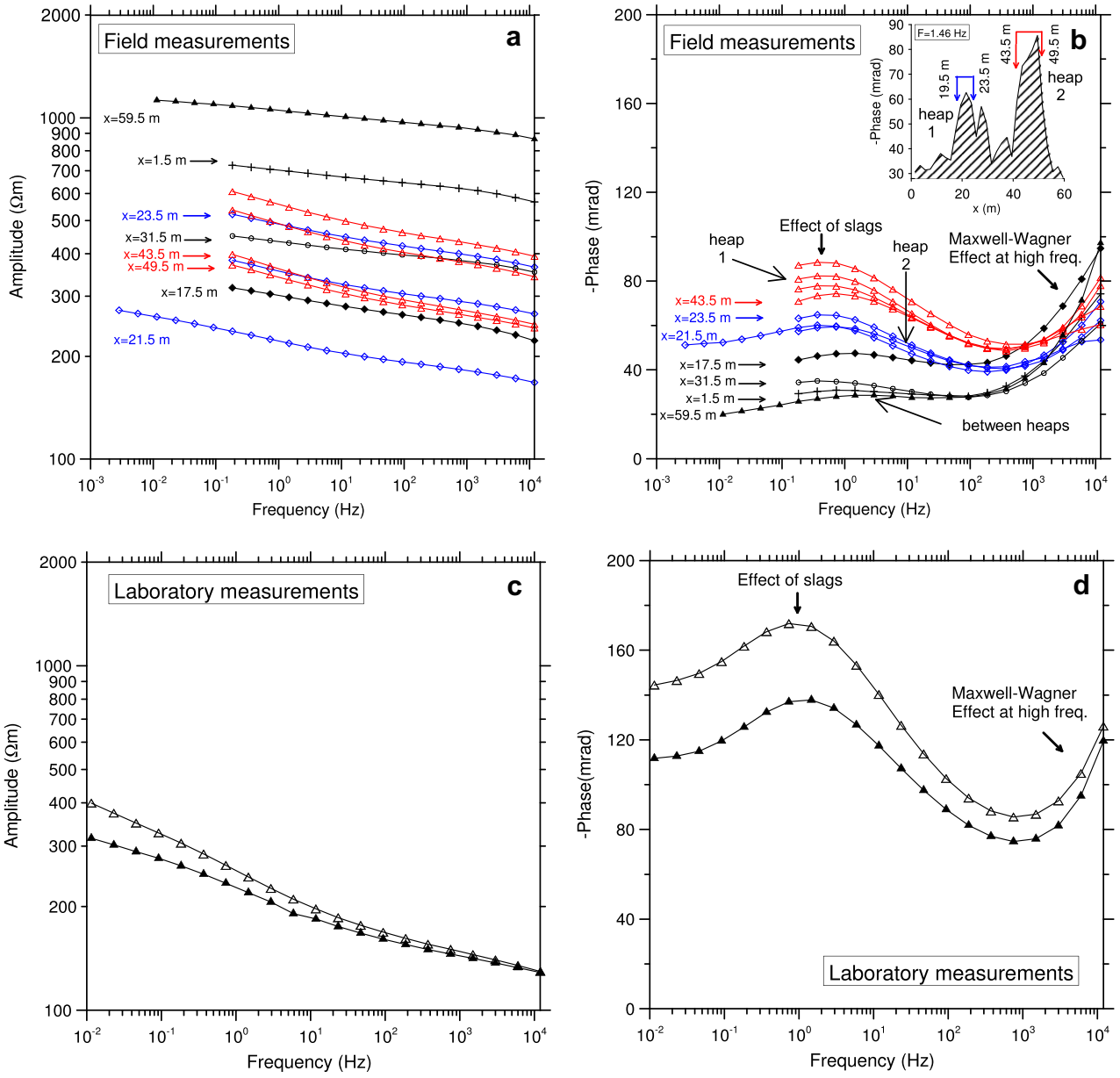

Fig. 7. Full set of spectral curves corresponding to the SIP profile and to two slag concentrates taken back to the laboratory: (a) amplitude along the profile on the field; (b) phase along the profile on the field; (c) amplitude of two samples from heap 2, measured in the laboratory; (d) phase of two samples from heap 2, measured in the laboratory.

$n = 1, 2, 3, 5$ and 8 have been used, to save time. We did have multi-wires at our disposal, but preliminary tests showed us that some inter-wire coupling was present and that measurements became spurious when $n \geq 3$ (this because the signal decreases as $1/(n\cdot(n+1)\cdot(n+2))$, while the EM coupling is more or less constant).

Fundamentally, the IP measurement protocols are strictly equivalent to those used for electrical methods. With a commercial IP measuring apparatus, one can consider the resistivity to be a by-product of the IP method rather than the reverse. However, in multi-electrode IP tomography, special care must be devoted to reducing electromagnetic coupling, ideally by using a dipole–dipole array with separate cables for the injection and the measurements.

In the RES2DINV and RES3DINV programs, Loke et al. (2006) applied a classical calculation technique to IP. The technique involved a perturbation of the resistivity, using an idea developed by Seigel (1959). Some misprints in Seigel's paper are corrected in Bertin and Loeb (1976, pp. 254–256). Additional details can be found in Luo and Zhang (1998, pp. 92–103).

Fig. 8 shows the full set of measurements obtained for this slag heap and its surroundings. It associates a mapping surface with RES2DINV cross-sections (2D profile providing a vertical tomography), one expressed in terms of resistivity and the other in terms of chargeability. The corroboration of these measurements with the geomatic information obtained from the archaeological excavations is provided in Fig. 9a for resistivity, and Fig. 9b for chargeability.

The resistivity provides, as usual, a signal representing the water and clay content. To the right, the chart includes the geoelectrical track of a watercourse thalweg. At the centre of the cross-section, the resistant area corresponds to a wall against which the slag heaps are butted.

The heap is not detected as such on the resistivity images, since various heterogeneities mask its presence. It should be noted that the slag heap is not solid, but is relatively scattered, although

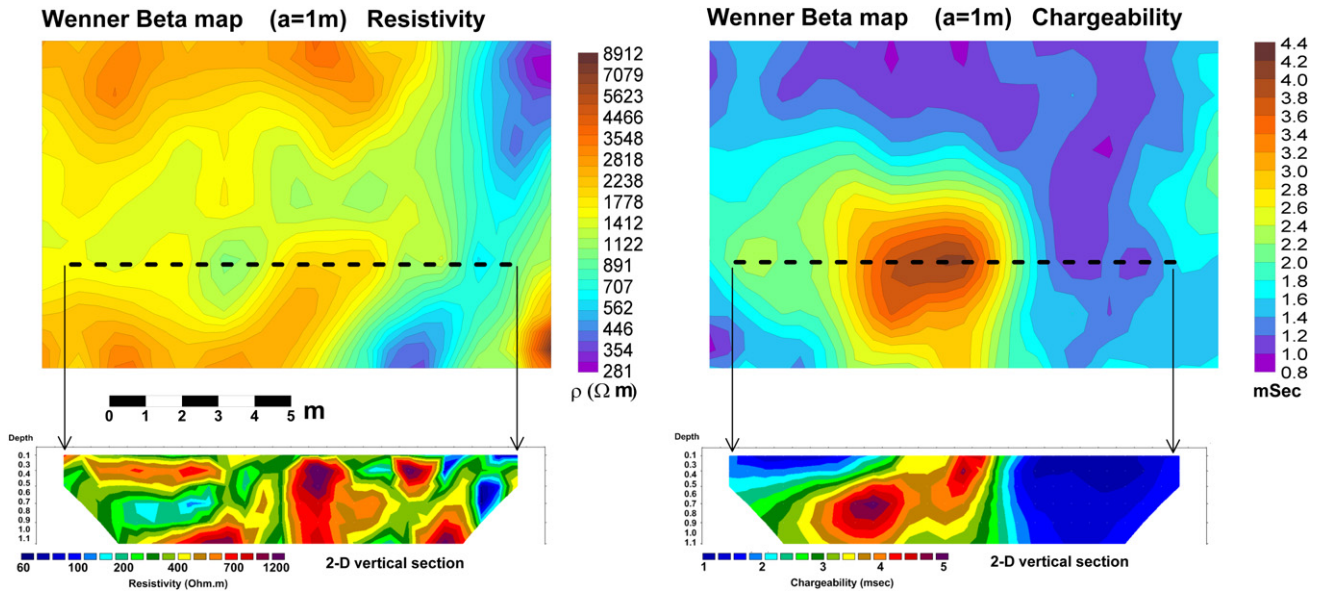

Fig. 8. Resistivity and experimental chargeability maps, as well as vertical cross-sections for the same parameters, determined along a locus shown by the dotted lines on the maps.

confined. The maximum concentration is 40%, a value which is found from the maximum chargeability observed on the cross-section (i.e., 5 ms) on the calibration curve.

In Fig. 9b, on the other hand, the heap is revealed spectacularly well on the map and the partial chargeability cross-section: the measurement procedure is found to clearly discriminate slags and to provide a good representation of their concentration. It is important to note that, apart from the general slope, the variation of the relief in those areas is not significant and thus no topographic correction was required.

4.3. Estimation of the slag mass based on geophysics

The inversion-derived chargeabilities are quantities identical to those one could measure by taking field samples, as in the case of calibrations. Of course, the geophysical image is smoothed, which has the effect of 'smearing' the real distribution. The value of the integral is however conserved by this filter, because the nature of the measurement itself involves an 'averaging' of the underground slag concentrations. This is the reason for which, in order to estimate the slag concentration, the calibration expression can be used directly by applying equation [16], from which:

$$C(x,\ y,\ z) = \frac{M_{t_1,t_2}(x,\ y,\ z) - \beta}{\alpha}.$$

An estimator is thus proposed, of the form:

$$\text{Total slag mass} = \rho_{\text{slag}} \iiint_{\text{prospect}} C(x,\ y,\ z)\text{dxdydz} \qquad (17)$$

In the present case, we do not have a full 3D image, but only a hypothetical inverted 2D cross-section (whereas the body is in 3D) and a flat, non-tomographic image measured at the surface. It is thus only possible to make a very approximate estimation, at best to a value within a factor of 2, by proceeding 'by hand' and using graphs, rather than by calculation.

By simplifying, from these graphs, the heap to a 3-axis ellipsoid with semi-axes of: $a = 3$ m, $b = 2$ m, and $c = 0.5$ m, the volume of interest is provided by the formula $V_{\text{slag}} = \pi abc$, i.e., 9.5 m^3. If one considers the density of slags to be close to the density of soil (which is the case here as shown by measurements of these densities), the mass concentration can be associated with a volume concentration. We attribute a slightly extrapolated chargeability of the order of 5 ms to this volume, so that, according to the calibration curve, we obtain a relative concentration of 0.4. By assuming a density close to 2, the total mass of the slags on this area of the map would be of the order of $9.5 \times 0.4 \times 2 = 7.6$ tons. According to our colleagues Eschenlohr and Serneels (1991), Serneels (1993) and Leroy (2001), who estimate the metal production based on slag quantity, its chemical composition and the nature of the ore, these 7.6 tons of slag are indicative of an iron production between 5.5 and 6.9 tons of commercial iron.

5. Validation, interpretation and discussion

In order to validate this estimation, which is based on a laboratory calibration, it is useful to compare the concentrations derived from maps and geophysical cross-sections with the concentrations measured in several terrain surveys. The latter are indicated by the grey shaded areas in Fig. 9.

In fact, following the geophysical studies, the excavation of the southern part of the slag heap required the manual removal of nearly 90 m^3 of sediment. During this work, three column samples were collected from the full thickness of the deposit, thereby generating three large samples of the terrain, from which the effective concentrations could be compared with those derived from the geoelectric chargeability.

The first 30 cm of sedimentation were not taken into account, since they were removed with an excavator during the preliminary surface removal activities. This section corresponds to a layer of topsoil covering the slag heap, which did not contain slags.

To determine the percentage of slags in the sediments, the total mass was measured before being sifted with water. The material was separated into three granulometric classes: one larger than 3 cm, a second one between 3 cm and 5 mm, and a third between 5 and 2 mm. The material with a fraction smaller than 2 mm was eliminated. After drying, the coarsest granulometric fraction was sorted. The slags, in a broad sense, were separated. However, for the intermediate and fine fractions, *in situ* sorting could not be carried out, and samples were thus collected. It is estimated that the mass of the slags contained in the latter was close to 20%. The sorted

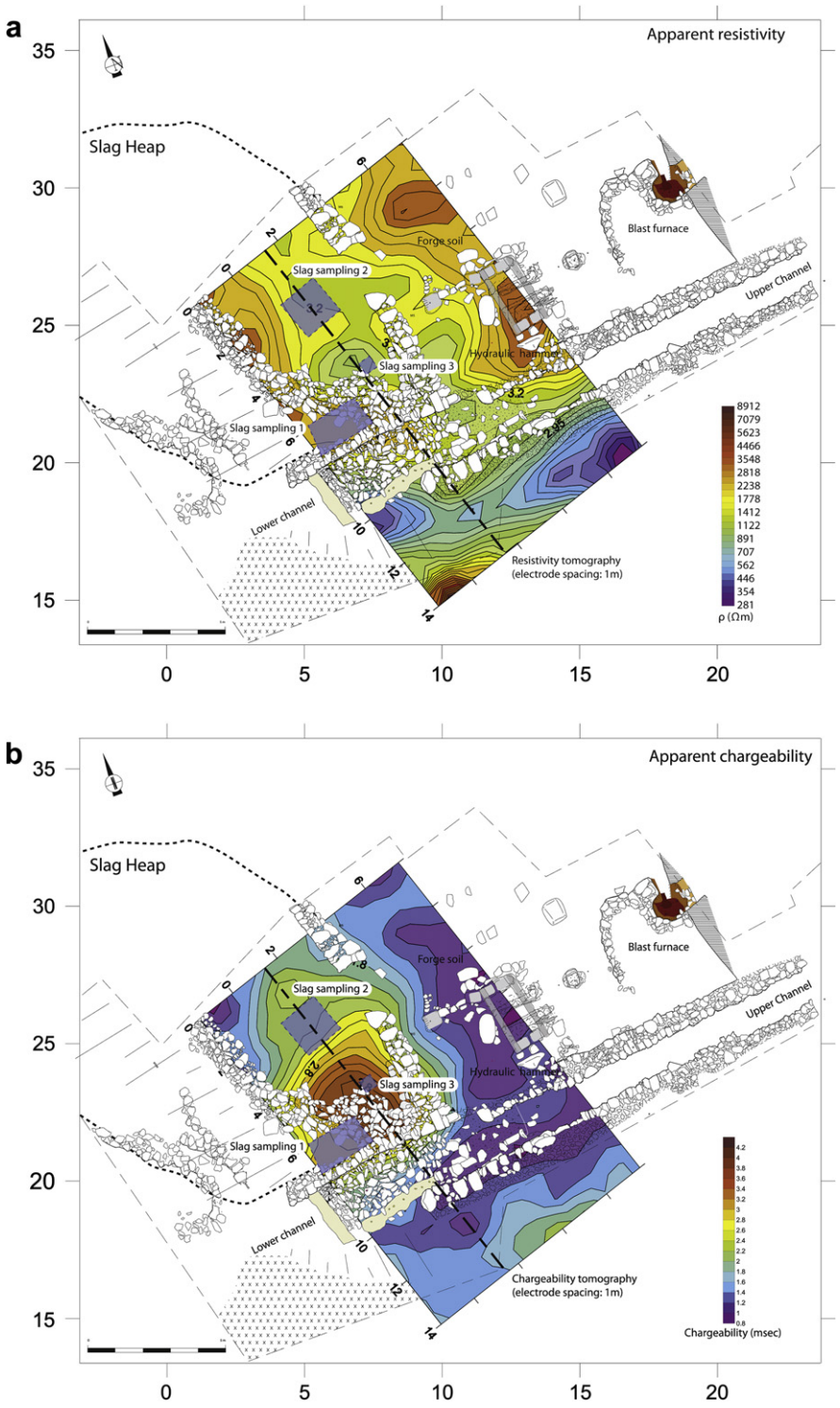

Fig. 9. Superimposition of the results of the archaeological excavation with apparent resistivity and apparent chargeability maps. The grey shaded areas correspond to the location of the excavations, from which all of the sediments were removed for analysis, thereby enabling the calibration curve to be validated.

material was then weighted again. This led to obtaining one value of the mass concentration which accounts for slags greater than 3 cm in size, and to a second value which includes slags of all dimensions. Although they were taken in order to determine the composition of the slag heap, the three samples came from the exploration surface. They represent, alone, more than 4.4 tons of sediment. Table 1 summarizes this data.

It should be noted that the slag heap, identified according to geological criteria, covers a larger surface area than the one studied using induced polarization prospection (see photograph – Fig. 10). The slag layers cover approximately 100 m^2. An estimation of the volume of approximately 100 m^3 of this heap had already been proposed by Bonnamour et al. (2007). The excavation showed that the densest layers of scrap covered 90 m^2, whereas the induced

Table 1
Quantitative data obtained after weighing, washing and sorting of three representative samples collected from the slag heap.

	Sample 1	Sample 2	Sample 3	**Total**
Volume in m^3	0.68	1.25	0.25	**2.18**
Mass in kg	1814	2369	282	**4465**
Sediment (<2 mm) in kg	697	1104.4	143.8	**1945.2**
Stones in kg	254	93	6.7	**353.7**
Slags in kg	326	493.27	51	**870.26**
Ave. particle size in kg	474	595.5	72.1	**1141.6**
Particle size (fine) in kg	61	70	7.96	**138.96**
Other (charcoal, root etc.)	2	12.8	0.5	**30.5**
Global density	2.6	1.9	1.12	**2.05**
Mass % of coarse slag (≥3 cm)	17.97	20.82	18.08	**19.49**
Mass % of slags (≥2 mm)	23.87	26.44	23.76	**25.23**

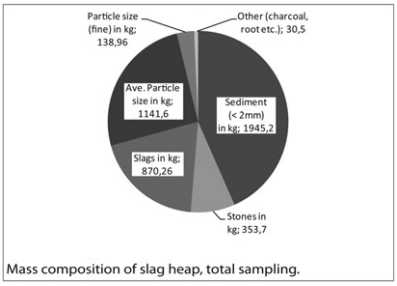

Mass composition of slag heap, total sampling.

polarization map covers the slag heap as well as the forge and the hydraulic channel.

The first piece of information revealed is of course the heterogeneity of the layers inside the slag heap itself. This information was already available, but difficult to interpret, using the chargeability map. The density can vary by a factor of more than 2. On the other hand, the estimation of a mean density of 2 is validated. Similarly, the order of magnitude of slag concentration, expressed as N% mass, fits with our observations following the excavation (between 20 and 25% mass).

It thus became possible to compare the mass concentrations obtained as a result of excavation with those determined from chargeability values derived from the map and the chargeability cross-section, which are then converted using the calibration curve shown in Fig. 4.

Fig. 10. Photograph of the excavated area, and superimposition of the IP geophysical map area obtained before excavation.

5.1. Concerning sample 1

The slag mass concentration (direct measurement) is between 18 and 24%. The chargeability value is between 2.8 and 3 ms on the Wenner Beta map. The sounding depth was designed to study the centre of the buried heap, which allows the apparent chargeability to be likened, roughly speaking, to the real chargeability. Following conversion using the calibration curve, this leads to a concentration in the range of 19 and 21%. This first result is very encouraging.

5.2. Concerning sample 2

This heap was deeper, and the Wenner Beta map provides apparent chargeabilities which are slightly lower than the real values. It is preferable to make use of the inverted cross-section, which really crosses the heap.

The archaeological sample provides a value between 21 and 26% in terms of mass concentration, whereas the IP measurement leads to an estimation in the range of 23 and 30%. Despite this small difference, the values correspond.

5.3. Concerning sample 3

The sampling indicates a slag mass between 19.5 and 25%, whereas geophysical analysis shows a range between 25 and 30%. Although this outcome seems less satisfactory, it should be noted that the situation is somewhat different in this case. For samples 2 and 3, an excavator was used initially. Although this step would have had no consequences for sample 2, since the slags were buried deeper down, the removal of the surface layer may have touched the top of heap no. 3, thereby leading to an underestimation of the slag mass.

Finally, these comparisons validate the interpretation and conversion of the slag concentration chargeability maps. The differences between measured and derived concentrations suggest that a suitable conversion of a geophysical slag mass map could enable the latter to be identified, in a given area. This could be achieved to within an accuracy of 30%, perhaps even 20%, without the need for surface layer removal or systematic excavations.

6. Discussion – perspectives

These results provide a strong motivation for further studies of the potential of this palaeometallurgical technique, and raises the question of what other avenues could be explored.

From the point of view of methodologies, 3D studies should be implemented systematically. It can be noted that 3D sounding may require only a series of parallel electric panels (i.e., a series of 2D measurements), with a spacing between profiles equal to 1 or 2 times the inter-electrode separation. Indeed, linear panels are sensitive to lateral structures, just as they are sensitive to structures situated directly above the profile. A set of parallel panels can thus probe the 3D information needed for a 3D inversion. An alternative method could be based on the use of surface maps, established at several sounding depths.

Once the cross-sections or maps have been inverted, they can be directly converted into slag concentration cross-sections, and by integrating these, deriving the total mass of the buried slags would be straightforward.

From the point of view of our understanding of slags, it would be very useful to confirm this type of affine relation (such as $M_{t1,t2} = \alpha C + \beta$) for different types of slag, and to derive the corresponding constants. It would also be useful to examine the time constants used, in order to determine whether they can be used as a discriminating parameter. To this effect, all recent studies confirm

the results of Pelton et al. (1978), in which his Fig. 6 indicates that τ is proportional to the square of the size of the grains (on his diagram, this is shown by two decades in the value of τ corresponding to one decade in grain size).

Of the various studies to be undertaken, one of the most important is certainly that of associating IP responses with the nature of the particles and minerals producing the observed signal. For that, it would be possible to separate the mineral phases of slags, and then to produce as many artificial mediums as there are phases to be tested. This could be achieved, for example, by reincorporating the latter into soil of the type found at the site, or into a neutral medium such as kaolinite. The four main candidates are certainly: metallic particles, sulfides, magnetite, and charcoal residues.

From the instrumental point of view, and assuming the time constants to be mostly greater than 200 ms, it would be possible to devise fast devices dedicated to mapping. They could be operated either in the time domain, with integrations over short time intervals and current cut-off, or in the frequency domain, with or without simultaneous measurements at two frequencies – one at a low frequency (not more than a few Hz) and the other at a higher frequency (around 100 Hz), and making use of 'PFEs'.

The device described on the website.

http://www.l-gm.de/English/Resistivity_Meters/resistivity_meters.html is probably well suited to these objectives, but we have not had the opportunity to test it.

7. Conclusions

Currently, slag masses are used to derive the quantities of metal produced at a given site. The estimation of the latter is affected by several approximations, beginning with the quantification of slags. This quantity is nevertheless essential to the analysis of the history of metal-working techniques, and with the associated economic history. Using a method developed in iron archaeometallurgy, we will be able to estimate with accuracy the iron production at the Castle-Minier *mouline* from the 16th century. At the same site, a slag heap issued from a manufacturing forge exists as well. In the future, we will apply the same methodology to it, and add a 3D model. Moreover, as the excavations continue, we will also classify slag manufacturing based on geophysical measurements and extensive archaeological sampling.

We have shown that the induced polarization technique is particularly useful for the quantitative characterization of slag heaps. Provided that laboratory calibrations and *in situ* measurements similar to those obtained by electrical techniques are used, this method enables the mass of metallurgical remains to be estimated. This opens up new opportunities for the quantification of scrap resulting from the production of iron, but probably also from other metals, such as copper, silver and lead.

In the field of archaeology alone, numerous explorations carried out in both ancient and medieval iron-making districts have led to the localization of numerous slag heaps. The exhaustive excavation of all of these is impossible, and in most cases the archaeologist has to resort at best to limited soundings, at worst to a visual estimation of the volume. The routine use of this technique will lead to the reassessment of the mass of scrap resulting directly from the production of the most commonly used metal in Europe.

Acknowledgments

The two reviewers have provided very constructive suggestions to improve the manuscript structure and content. We thank Thilo Rehren for having managed the successive versions of the text. Special thanks to Raul Carstocea for his help with the final language editing.

Appendix

Partial chargeability of an early time window, Cole–Cole model.

Pelton et al. (1978) provided a formula for the decreasing potential of the injected current after the cut-off, as follows:

$$V_{\text{Pelton}}(t) = \rho_0 m \sum_{n=0}^{\infty} \frac{(-1)^n \left(\frac{t}{\tau}\right)^{nc}}{\Gamma(1+nc)} \tag{18}$$

where ρ_0 is the resistivity, m the chargeability, τ the time constant and c the 'cementation factor' in the Cole–Cole model. Γ is the gamma Euler function with $\Gamma(z+1) = z\Gamma(z)$. This series converges in any case, but when $t >$ tau it is better to employ the one provided by Hilfer (2002).

Since we use the normalized potential, with respect to the potential before the cut-off, we are concerned only with:

$$V(t) = m \sum_{n=0}^{\infty} \frac{(-1)^n \left(\frac{t}{\tau}\right)^{nc}}{\Gamma(1+nc)} \tag{19}$$

Integration between t_1 and t_2 yields:

$$\begin{aligned} M_{t_1,t_2} &= \int_{t_1}^{t_2} V(t)\mathrm{d}t = m \sum_{n=0}^{\infty} \frac{(-1)^n}{\Gamma(1+nc)} \left(\frac{1}{\tau}\right)^{nc} \int_{t_1}^{t_2} t^{nc}\mathrm{d}t \\ &= m \sum_{n=0}^{\infty} \frac{(-1)^n}{\Gamma(2+nc)} \tau \left[\left(\frac{t_2}{\tau}\right)^{nc+1} - \left(\frac{t_1}{\tau}\right)^{nc+1} \right] \end{aligned} \tag{20}$$

Considering the two first terms in this expansion only leads to:

$$\begin{aligned} M_{t_1,t_2} &= m(t_2 - t_1) - \frac{m\tau}{\Gamma(2+c)} \left[\left(\frac{t_2}{\tau}\right)^{c+1} - \left(\frac{t_1}{\tau}\right)^{c+1} \right] \\ &\quad + (\text{remaining higher orders of } t/\tau). \end{aligned} \tag{21}$$

Remembering that $c > 0$ and assuming $t_1 < t_2 << \tau$ leads to the approximation:

$$M_{t_1,t_2} \cong m(t_2 - t_1) \tag{22}$$

In the following, we compute a numerical example relevant to the present study. We assume the following constants: $\tau \approx 1$ s, $t_1 = 0.01$ s, $t_2 = 0.03$ s, and $c = 0.8$. Numerically, the ratio between the second term and the first one is:

$$|r| = \frac{\frac{1}{\Gamma(2.8)} \left[\left(\frac{0.03}{1}\right)^{1.8} - \left(\frac{0.01}{1}\right)^{1.8} \right]}{(0.02)} = 0.047 \tag{23}$$

This means that an error of about 5% is made on m by applying this simplified formula.

References

Aspinal, A., Lunam, J., 1968a. Induced polarization as a technique for archaeological surveying. Prospezioni Archeologiche 3, 91–93.
Aspinal, A., Lunam, J., 1968b. An induced polarization instrument for the detection of near-surface features. Prospezioni Archeologiche 5, 67–75.
Aspinal, A., Gaffney, C., Schmidt, A., 2008. Magnetometry for Archaeologists. Altamira Press, ISBN 0759113483, 224 p. 9780759113480.
Bailly-Maitre, M.-C., Bruno-Dupraz, J., 1994. Brandes-en-Oisans, la mine d'argent des Dauphins (XII-XIVe s.) Isère, D.A.R.A. no9, Lyon, 170 p.
Benoit, P., 1997. La mine de Pampailly XVe-XVIIIe siècles, Brussieu Rhône, D.A.R.A. no14, Lyon, 137 p.

Bertin, J., Loeb, J., 1976. Experimental and theoretical aspects of induced polrization. In: Loeb, J. (Ed.), Vol. 2: Macroscopic and Microscopic Theories. Edts Geopublication Associates, ISBN 3-443-13010-0.
Bonnamour, G., Florsch, N., Téreygeol, F., 2007. Les prospections des ferriers de Castel-Minier: approche interdisciplinaire. ArcheoSciences Revue d'Archéométrie 31, 37–44.
Domergue, Cl, Leroy, M., 2000. Mines et métallurgie en Gaule, recherches récentes. Gallia 57, 1–158.
Cole, K.S., Cole, R.H., 1941. Dispersion and absorption in dielectrics. I. Alternating current characteristics. Journal of Chemical Physics 9, 341–351.
Cosenza, Ph., Ghorbani, A., Florsch, N., Revil, A., 2007. Effects of drying on the low-frequency electrical properties of Tournemire argillites. Pure and Applied Geophysics. doi:10.1007/s00024-007-0253-0.
Dabas, M., Jolivet, A., Tabbagh, A., 1992. Magnetic susceptibility and viscosity of soils in a weak time varying field. Geophysical Journal International 108, 101–109.
Decombeix, P.-M., Fabre, J.-M., Tollon, F., Domergue, Cl, 1998. Evaluation du volume des ferries romains du domaine des Forges (Les Martys, Aude), de la masse de la masse de scories qu'ils renferment et de la production de fer correspondante. ArcheoSciences Revue d'Archéomètrie 22, 77–90.
Dey, A., Morrison, H.F., 1973. Electromagnetic coupling in frequency and time domain induced polarisation surveys over multilayered earth. Geophysics 38, 380–405.
Dias, C.A., 2000. Developments in a model to describe low-frequency electrical polarization of rocks. Geophysics 65, 437–451.
Dillmann, P., Téreygeol, F., Verna, C., 2006. Premières analyses métallographiques des produits sidérurgiques trouvés sur le site médiéval de Castel-Minier (Aulus-les-Bains, 09). ArchéoSciences Revue d'Archéométrie 30, 7–14.
Eschenlohr, L., Serneels, 1991. Les bas fourneaux mérovingiens de Boécourt (JU/Suisse). Cahier d'archéologie jurassienne 3, Porrentruy, 144 p.
Fasnacht, W., 1999. Agia Varvara-Almyras: ein Fundpaltz des Kupferberghaus und der VerhUttung auf Zypern. In: Kupfre für Europa, Bergau und Handel auf Zupern. Wachholtz Verlag, Neumünster.
Florsch, N., Llubes, M., Téreygeol, F., Ghorbani A, Roblet, P., 2008. Quantification of buried slag volumes by using non-invasive geophysical methods. In: Proceedings of the 1st EARSeL International Workshop On "Advances in Remote Sensing for Archaeology and Cultural Heritage Management" Rome 30 September–4 October, 2008.
Fuoss, R.M.D., Kirkwood, J.G., 1941. Electrical properties of solids. VIII. Dipole moments in polyvinyl chloride-diphenyl systems. Journal of the American Chemical Society 63, 385–394.
Ghorbani, A., Camerlynck, C., Florsch, N., Cosenza, P., Revil, A., 2007. Bayesian inference of the Cole–Cole parameters from time- and frequency-domain induced polarization. Geophysical Prospecting 55, 589–605. doi:10.1111/j.1365-2478.2007.00627.x.
Ghorbani, A., Cosenza, Ph., Ruy, S., Doussan, C., Florsch, N., 2008. Non-invasive monitoring of water infiltration in a silty clay loam soil using Spectral Induced Polarization. Water Resources Research 44, W08402. doi:10.1029/2007WR006114.
Ghorbani, A., Cosenza, P., Revil, A., Zamora, M., Schmutz, M., Florsch, N., Jougnot, D., 2009b. Non-invasive monitoring of water content and textural changes in clay-rocks using Spectral induced Polarization: a laboratory investigation. Applied Clay Science 43 (3–4), 493–502. March 2009.
Ghorbani, A., Camerlynck, C., Florsch, N., 2009a. CR1Dinv: a Matlab program to invert 1D spectral induced polarization data for the Cole–Cole model including electromagnetic effects. Computers & Geosciences 35, 255–266.
Guéguen, Y., Palciauskas, V., 1992. Introduction à la physique des roches. Herman Edts, Paris.
Hilfer, R., 2002. Analytical representations for relaxation function of glasses. Journal of Non-Crystalline Solids 305, 122–126.
Hohmann, G.W., 1973. Electromagnetic coupling between grounded wires at the surface of a two-layer earth. Geophysics 38, 854–863.
Ingeman-Nielsen, T., Baumgartner, F., 2006. CR1Dmod: a Matlab program to model 1D complex resistivity effects in electrical and EM surveys. Computers & Geosciences 32, 1411–1419.
Le Borgne, E., 1960. Influence du feu sur les propriétiés magnétiques du sol et du granite. Annals of Geophysics 16, 159–195.
Leroy, B., 1972. Théorie monétaire et extraction minière en Navarre vers 1340. Revue de Numismatique, 105–123.
Leroy, M., 2001. La sidérurgie en Lorraine avant le haut fourneau, l'utilisation du minerai de fer oolithique en réduction directe, monographie du CRA, no18, Cnrs édition, 205 p.
Leroy S., 2010. Circulation au Moyen Âge des matériaux ferreux issus des Pyrénées ariégeoises et de la Lombardie, Thèse de 3e cycle, Université de Belfort, vol 2.
Loke, M.H., Chambers, J.E., Ogilvy, R.D., 2006. Inversion of 2D spectral induced polarization imaging data. Geophysical Prospecting 54, 287–301.
Luo, Y., Zhang, G., 1998. Theory and application of spectral induced polarization. In: Geophysical Monograph Series (8). Society of Exploration Geophysicists, Tulsa, p. 171.
Malus J., [1600], 1990. Recherche et Descouverte des mines des montagnes Pyrénées, réédition A. Bourneton, Toulouse, 110 p.
Meyer, C., Ullrich, B., Barlieb, C.D.M., 2007. Archaeological questions and geophysical solutions: ground-penetrating radar and induced polarization investigations in Munigua, Spain. Archaeological Prospection 14, 202–212.
Millett, F.B., 1967. Electromagnetic coupling of collinear dipoles on a uniform half-space. In: Mining Geophysics, vol. II. Society of Exploration Geophysicists, Tulsa, pp. 401–419.
Nordsiek, S., Weller, A., 2008. A new approach to fitting induced polarization spectra. Geophysics 73, F235–F245. doi:10.1190/1.2987412.
Panissod, C., Dabas, M., Hesse, A., Jolivet, A., Tabbagh, J., Tabbagh, A., 1998. Recent developments in shallow-depth electrical and electrostatic prospecting using mobile arrays. Geophysics 63, 1542. doi:10.1190/1.1444450.
Parasnis, D.S., 1997. Principles of applied geophysics, fifth ed. Chapman and Hall Edts, ISBN 0-412-80250-3. or 0-412-64080-5.
Pelton, W.H., Ward;, S.H., Hallof, P.G., Sill, W.R., Nelson, P.H., 1978. Mineral discrimination and removal of inductive coupling with multifrequency IP. Geophysics 43, 588–609.
Revil, A, Florsch, N., 2010. Determination of permeability from spectral induced polarization in granular media. Geophysical Journal International 181, 1480–1498, doi:10.1111/j.1365-246X.2010.04573.x
Schlumberger, F.C., 1920. Etude sur la prospection électrique du sous-sol. Gauthier-Villars, Paris.
Schön, J.H., 2004. Physical Properties of Rocks: Fundamentals and Principles of Petrophysics. Pergamon Press. ISBN-10: 008044346X, ISBN-13: 978-0080443461.
Scollar, I., Tabbagh, A., Hesse, A., Herzog, I., 1990. Archaeological Prospecting and Remote Sensing, 696 p. Cambridge University Press. ISBN-10: 052132050X/ISBN-13: 978-0521320504.
Seigel, H., 1959. Mathematical formulation and type curves for induced polarization. Geophysics 24, 547–565.
Seigel, H., Nabighian, M., Parasnis, D., March 2007. The early history of the induced polarization method. The Leading Edge 26 (3), 312–321. doi:10.1190/1.2715054.
Serneels, V., 1993. Archéométrie des scories de fer. Recherche sur la sidérurgie ancienne en Suisse occidentale. Cahier d'archéologie romande, Laussanne, no61 240 p.
Shin, F.G., Yeung, Y.Y., 1988. On the connection between the spectral shape function for dielectric susceptibility and a non-linear differential equation. Journal of Materials Science Letters 7, 1066–1067. doi:10.1007/BF00720829.
Soterel, G., 1340. Arch. de Navarre, diputacion Foral, Pampelune, Série Document des comptes, Caj. 24 no38, I, 1340, fol. 6.
Tabbagh, A., Dabas, M., 1996. Absolute magnetic viscosity determination using time domain electromagnetic devices. Archaeological Prospection 3, 92–100.
Telford, W.M., Geldart, L.P., Sheriff, R.E., 1990. Applied Geophysics, second revised ed. Cambridge University Press, ISBN-10: 0521339383 / ISBN-13: 978-0521339384 792 p.
Téreygeol, F., 2002. Frümittelalterlicher Bergbau und Silberproduktion von Melle in Frankreich. Der Anschnitt, Zeitschrift für Kunst und Kultur im Bergbau 54 (6), 253–266.
Téreygeol, F., 2009. Le Castel-Minier (Aulus-les-Bains), rapport intermédiaire, tapuscrit. Service Régional de l'Archéologie Midi-Pyrénées, 91 p.
Téreygeol F., Arles A., Foy E., Florsch N., Llubes M. Dosages par fluorescence X portable d'ateliers médiévaux de production des métaux non-ferreux: les exemples de Castel-Minier et d'Agnesserre (Aulus-les-bains, 09), Archéosciences, Revue d'Archéométrie. in press
Thiesson, J., Tabbagh, A., Flageul, S., 2007. TDEM magnetic viscosity prospecting using Slingram coil configuration. Near Surface Geophysics 5, 363–374. doi:10.3997/1873-0604.2007018.
Titov, K., Tarasov, A., Llyin, Y., Seleznev, N., Boyd, A., 2009. Relationships between induced polarization relaxation time and hydraulic properties of sandstone. Geophysical Journal International 180, 1095–1106. doi:10.1111/j.1365-246X.2009.04465.x.
Ullrich, B., Günther, T., Rücker, C., 2007. Electrical resistivity tomography methods for archaeological prospection. In: Proceedings of the 35th International Conference on Computer Applications and Quantitative Methods in Archaeology (CAA). Berlin, Germany, April 2–6, 2007.
Verna, C., 1996. Une nouvelle page de l'histoire des mines d'argent européennes: le cas des Pyrénées centrales (XIV^{e} – XV^{e} siècle). Bulletin annuel de la Société Ariégeoise Sciences Lettres et Arts, 201–232.
Verna, C., 2001. Le temps des moulines, Fer, technique et société dans les Pyrénées centrales (XIIIe-XIVe siècles). Publications de la Sorbonne, Paris, 425 p.
Wait, J.R., Gruszka, T.P., 1986. On electromagnetic coupling removal from induced polarization surveys. Geoexploration 24, 21–27.
Weller, A., Brune, S., Hennig, T., Kansy, A., 2000. Spectral induced polarization at a medieval smelting site. In: Proceedings of the 6th Meeting, Environmental and Engineering. Geophysics (EEGS-ES) EL11 (Bochum 2000).
Wynn, J.C., Zonge, K.L., 1977. Electromagnetic coupling. Geophysical Prospecting 25, 29–51.
Yeung, Y.Y., Shin, F.G., 1991. Pulse response functions of dielectric susceptibility. Journal of Materials Science 26, 1781–1787.